RESEARCH ARTICLE
Cytoskeleton, Month 2014 00:00–00 (doi: 10.1002/cm.21197)

Microtubule Orientation and Spacing Within Bundles is Critical for Long-Range Kinesin-1 Motility

Leslie Conway,[1] Michael W. Gramlich,[1] S. M. Ali Tabei,[2] and Jennifer L. Ross[1,2,3]*

[1]Department of Physics, University of Massachusetts Amherst, Amherst, Massachusetts
[2]Department of Physics, University of Northern Iowa, Cedar Falls, Iowa

Received 15 September 2014; Revised 3 November 2014; Accepted 4 November 2014
Monitoring Editor: Bruce Goode

Cells rely on active transport to quickly organize cellular cargo. How cells regulate transport is not fully understood. One proposed mechanism is that motor activity could be altered through the architecture of the cytoskeleton. This mechanism is supported by the fact that the cytoskeletal network is tightly regulated in cells and filament polarity within networks dictates motor directionality. For instance, axons contain bundles of parallel microtubules and all cargos with the same motor species will move in the same direction. It is not clear how other types of networks, such as antiparallel bundles in dendrites, can regulate motor transport. To understand how the organization of microtubules within bundles can regulate transport, we studied kinesin-1 motility on three bundle types: random-polarity bundles that are close-packed, parallel polarity bundles, and antiparallel polarity bundles that are spaced apart. We find that close-packed bundles inhibit motor motion, while parallel arrays support unidirectional motion. Spacing the microtubules with microtubule-associated proteins enhances run lengths. Our results indicate that microtubule bundle architecture dictates the motion of single motors and could have effects on cargo transport. © 2014 Wiley Periodicals, Inc.

Key Words: intracellular transport; long-range transport; traffic; motor protein; network organization

Introduction

Active transport of cellular cargo is an essential biological process for cell homeostasis. Fast and accurate localization of cellular cargo is achieved by active transport along cytoskeletal tracks powered by molecular motor enzymes. Unlike thermal diffusion, active transport is both fast and controllable. Further, diffusion-based transport of large vesicular cargo is extremely slow over long distances in the crowded space inside cells because large cargos become trapped [Massiera et al., 2007]. Active transport is especially important in large cells, such as neurons that have long, extended axonal, and dendritic compartments [Goldstein and Yang, 2000; Vale, 2003; Hirokawa and Takemura, 2005]. When active transport breaks down, the result is neurological and neuromuscular diseases such as Alzheimer's disease or amyotrophic lateral sclerosis, indicating the importance of a functional active transport system in neurons [Khatoon et al., 1992; Braak et al., 1994; Chevalier-Larsen and Holzbaur, 2006; Dixit et al., 2008; Perlson et al., 2010].

Long-distance transport in axons and dendrites uses the microtubule cytoskeletal network, with cargo carried by kinesin and cytoplasmic dynein motors. Microtubules are polarized filaments with a fast-growing plus-end and a slow-growing minus-end. Each type of motor walks unidirectionally on microtubules: kinesin toward the plus-end and cytoplasmic dynein toward the minus-end. Both use adenosine triphosphate (ATP) as an energy source. Many studies have focused on how the motors can be directly regulated by phosphorylation, associated light chains, through tug-of-war, or self-inhibition schemes [Hirokawa and Takemura, 2005; Hirokawa et al., 2010]. Prior studies have focused on the transport of motors and cargos along single microtubules. Yet, the cytoskeleton is a network of many microtubules. In the axons and dendrites of nerve cells, much of the microtubule network is in the form of bundles, whose organization is tightly regulated and developmentally controlled [Baas et al., 1988]. For instance, in early stages of neuron development, axons and dendrites both have parallel microtubule bundles with all the plus-ends pointing to the distal end and the minus-ends pointing to the cell body [Baas et al., 1988]. At later stages, dendritic microtubules develop a mixed polarity array of microtubules at the proximal region, while the distal end maintains a parallel array with plus ends distally oriented [Baas et al., 1988; Stepanova et al., 2003]. Could these different microtubule arrangements affect the localization of cargos inside the neuron?

Additional Supporting Information may be found in the online version of this article.

*Address correspondence to: Jennifer L. Ross, 666 North Pleasant Street, 302 Hasbrouck Laboratory, Amherst, MA 01003.
E-mail: rossj@physics.umass.edu

Published online 10 November 2014 in Wiley Online Library (wileyonlinelibrary.com).

In an effort to dissect the underlying mechanism by which the architecture of the cytoskeleton can regulate motor transport, we have tested the motility of single kinesin-1 motors along different architectures of microtubules using in vitro reconstitution experiments. We created bundles of microtubules with three different arrangements: (1) parallel orientation, (2) closed-packed randomly-oriented filaments created by crowding agents (inert polymers), (3) antiparallel orientation with spacing between the filaments created by microtubule-associated proteins (MAP65), and (4) antiparallel microtubules made by MAP65 spacers in the presence of inert polymers. For each of these bundles, we also perform control experiments testing the effects of the additives (inert polymers, MAP65) on single microtubules in order to test the effect of bundling and not the effect of the additives themselves. We use the kinesin-1 motor as a model processive motor to elucidate the rules that such an individual motor obeys. We carefully measured the association time, run length, and velocity of motors transporting along each type of bundle.

Interestingly, parallel bundles enabled run lengths and velocities in a single direction that were similar to the motility of kinesin-1 motors on single microtubules, suggesting that the extra binding sites afforded by the bundle did not enable motors to reattach to the track after dissociation. Unlike parallel bundles, randomly-oriented, close-packed bundles enabled reversals of motors along the bundle, but we found that the close packing of the microtubules inhibited the ability of the motors to have long run lengths in any one direction. Spacing the bundled microtubules by microtubule-associated proteins (MAPs) rescued the run length in a single direction compared to close-packed bundles. Our results indicate that MAPs, which are usually discussed as obstacles to long-range motor transport, can actually enhance transport by spacing apart microtubules of a bundle and allowing motors to overcome the larger hindrance from close packing of microtubule filaments.

We modeled the behavior of motor reversals on bundles using a simple model where the motors detach from a single filament and can reattach to the bundle on a different microtubule either in the same or the opposite direction. We compared the simulation to the experiment and found similar trends for the bundles that were spaced apart. Interestingly, the model was not capable of capturing the trends of motility for the close-packed bundles.

This study demonstrates new results as to how molecular motors transport on complex microtubule arrays. Specifically, it sheds light on how highly organized microtubule arrays may serve as an additional mechanism by which the cell could enable the regulation of cargo transport.

Results

Motility on Unipolar Bundles

In order to create parallel bundles for use in vitro, we took advantage of the cell machinery for creating parallel arrays. We isolated parallel microtubule bundles from neuronal-like cath.a-differentiated (CAD) cells, a mouse central nervous system catecholaminergic cell line that have been used as model neurons for intracellular transport studies [Qi et al., 1997; Verhey et al., 2001; Muresan and Muresan, 2012]. Upon serum starvation, these cells differentiate to form neurite-like processes. The extended processes have been shown by electron microscopy to contain parallel arrays of microtubules and neurofilaments. The cells are known to express MAP1b and LIS1 but no neuronal MAPs [Qi et al., 1997; Li et al., 2006; Bisig et al., 2009]. The post-translational state of microtubules in the CAD cell neurites is similar to brain-derived microtubules [Reed et al., 2006]. By adapting a previously determined method to preserve the actin cytoskeleton in keratocytes [Sivaramakrishnan and Spudich, 2009], we treated differentiated CAD cells with detergent and Taxol to simultaneously expose and stabilize the microtubule cytoskeleton while diluting away neurofilaments and endogenous MAPs (Figs. 1A and 1B).

Kinesin-1 motility on these parallel bundles was observed to be in a single direction, with all kinesin-1 motors moving toward the distal ends of the processes. We compared kinesin-1 motility properties on CAD cell bundles to motility on single microtubules polymerized in vitro (Fig. 1C). We quantified the association time, run length, and velocity of kinesin-1 motors on parallel bundles and single microtubules using the kymographs (Fig. 1C). The association time is the vertical displacement, the run length is the horizontal displacement, and the velocity is the inverse of the slope of the displacements in kymographs.

We quantified the percentage of kinesin motors that paused while walking along the microtubule to determine if the parallel bundles from cells displayed more obstacles. We distinguished a pause as a period of the motor's association that lasted at least two frames wherein the motor did not displace by more than 209 nm, the microscope resolution. The microscope resolution was estimated from the wavelength of detected light (510 nm) and the numerical aperture of the objective (1.49). We calculated the uncertainty as the standard error of proportion. Both data sets had similar percentages of motors that paused and were within the uncertainty of each data set (Fig. 1D; Supporting Information Table 1).

Plotting probability distribution functions (histograms), we can see that the association times and run lengths are both exponential decays (Figs. 2A and 2D). The data at short times (<1 s) and short run lengths (<1 μm) are under-represented because of our exposure time (0.5 s). We also display the cumulative probability distributions (Figs. 2B and 2E) because these representations display all the data and do not obscure data within bins that can be manipulated. These distributions also show similar trends and are all of the form:

$$y = 1 - A \exp\left(-\frac{x}{x_0}\right) \quad (1)$$

where A is an amplitude and x_0 is the characteristic decay constant (with units of time for association time data and

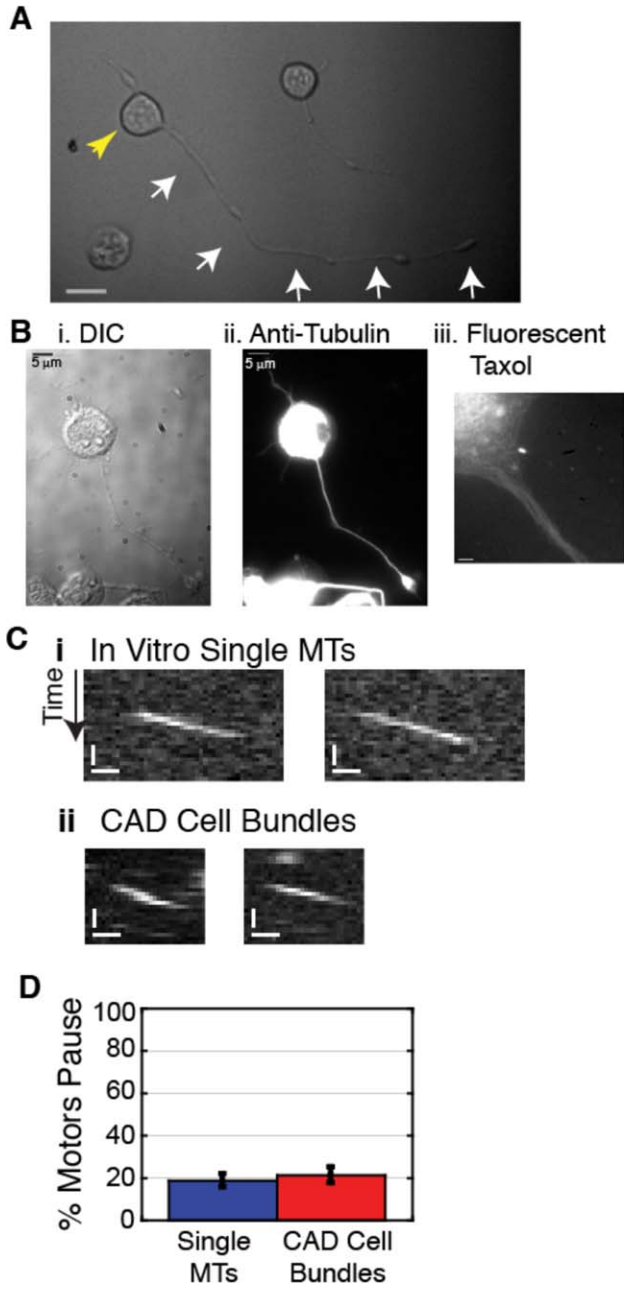

Fig. 1. Kinesin walking on parallel bundles made from CAD cells have same motility as on single microtubules. **A.** Transmitted light image of CAD cell after process formation is induced by serum starvation. The cell body (yellow arrowhead) and the long process (white arrows) are clearly seen for several cells (scale bar is 20 μm). **B.** Images of CAD cells in **i.** differential interference contrast (DIC) microscopy, **ii.** stained with antitubulin antibody, and **iii.** stained with Boron-dipyrromethene (bodipy)-labeled Taxol to image intact microtubule cytoskeleton after microtubule stabilization and membrane removal (scale bar is 3 μm). **C.** Representative kymographs of motors walking along **i.** single microtubules and **ii.** microtubule bundles from CAD cells. Time is positive going down (vertical scale bars are 2.5 s) and space is horizontal (horizontal scale bars are 0.5 μm). **D.** The percentage of kinesin motors that pause on single microtubules (blue bars) and parallel bundles from CAD cells (red bars). Error bars represent the standard error of proportion. [Color figure can be viewed in the online issue, which is available at wileyonlinelibrary.com.]

units of length for run length data). This function is expected for cumulative distributions of data that has exponentially decaying probability, and the amplitude is needed to compensate for the lack of short-time or short-distance data. We found the characteristic decay time by fitting the cumulative distribution functions to Eq. (1). Each data set was best fit by a single characteristic decay time. The cumulative distribution data for the run length of kinesin motors on parallel bundles had shorter run lengths than expected causing the exponential decay to not fit as well for data above 1.5 μm (Fig. 2E), but a double decay did not fit the data better. We compare the characteristic decay times for the cumulative association times and found the association time fits had a slight difference of 0.4 s (Fig. 2C; Supporting Information Table 1). This difference was larger than the uncertainty of either fit. The characteristic decay lengths for the run lengths were equivalent within the uncertainty of the fit (Fig. 2F; Supporting Information Table 1).

We observed that the velocity of motors on bundles from CAD cells displayed what appeared to be a sum of two Gaussians with significantly different mean values, whereas the velocity distribution for single motors on single microtubules was a single Gaussian (Fig. 3). We fit the data to a single Gaussian:

$$y = A \exp\left(-\frac{(x-x_0)^2}{2\sigma^2}\right) \tag{2}$$

where A is the amplitude, x_0 is the mean or center of the peak, and σ is the standard deviation of the distribution. For the parallel bundle data, we found that the single Gaussian had a mean of 0.35 ± 0.01 μm/s, but the fit was not as good ($\chi^2 = 0.0061$, $R^2 = 0.89$) as a fit of a sum of two Gaussians ($\chi^2 = 0.0048$, $R^2 = 0.91$). The fit of a sum of two Gaussians was best with means at 0.44 ± 0.05 μm/s and 0.24 ± 0.06 μm/s. The population of motors with the higher velocity had a similar average velocity as kinesin motors walking on single microtubules, which gave a mean value of 0.439 ± 0.005 μm/s when fit to a single Gaussian (Fig. 3; Supporting Information Table 1).

Motility on Random-Polarity Bundles

We created microtubule bundles in vitro that have randomly-oriented polarities using a macromolecular crowder, 5% 40 kD polyethylene glycol (PEG). Small angle X-ray diffraction showed that such bundles have microtubules that are close packed into hexagonal arrays [Needleman et al., 2004]. We determined that bundles average seven microtubules in cross-section in our assays by comparing the fluorescence intensity of bundles of microtubules to the fluorescence intensity of single microtubules (Fig. 4A).

When kinesin-1 motors walked along bundles made with PEG, we saw a significant number (34%) that reversed direction as characterized by a zigzag pattern in the kymographs, although the majority did not reverse direction

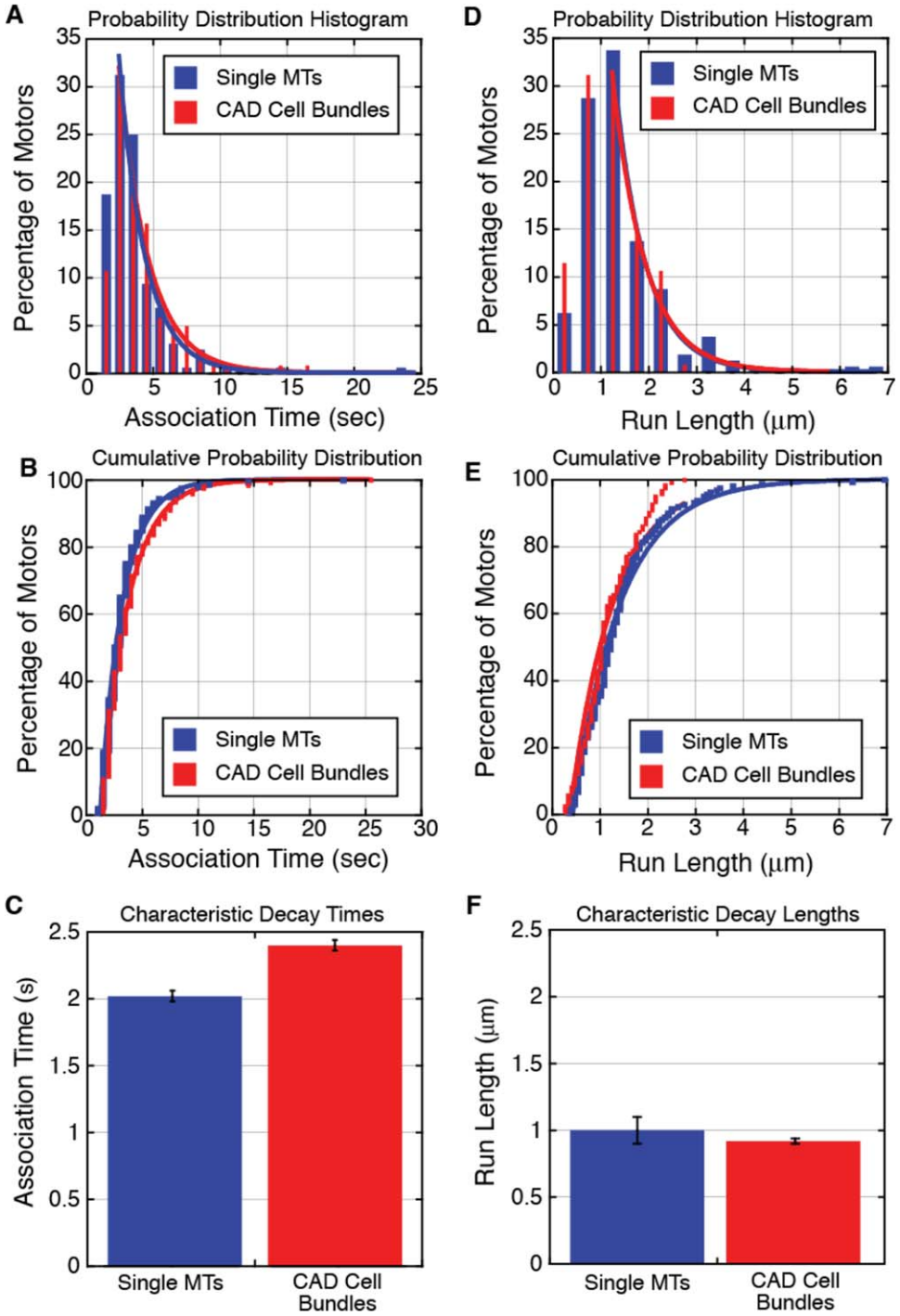

Fig. 2. Comparison of motility parameters for association time and run length for kinesin motors on parallel bundles. **A.** Normalized probability distribution histogram of the association times for kinesin motors on single microtubules (blue bars, $N = 160$) and parallel bundles (red bars, $N = 122$). Bin size is 1.0 s. The fit to times >1 s is an exponential decay $y = A^*\exp(x/x_0)$, where A is the amplitude and x_0 is the characteristic association time. The best fits for the kinesin motors on single microtubules (blue line, $A = 1.2 \pm 0.1$, $x_0 = 1.9 \pm 0.1$ s, $R^2 = 0.97$) and parallel bundles (red lines, $A = 0.98 \pm 0.7$, $x_0 = 2.2 \pm 0.1$, $R^2 = 0.98$) are shown. **B.** Normalized cumulative distributions of the association times of kinesin motors on single microtubules (blue squares) and parallel bundles (red squares). Cumulative distribution data were fit using Eq. (1) and best fits for motors on single microtubules (blue line, $A = 1.88 \pm 0.04$, $x_0 = 2.02 \pm 0.04$ s, $R^2 = 0.97$) and parallel bundles (red line, $A = 1.79 \pm 0.03$; $x_0 = 2.40 \pm 0.04$ s, $R^2 = 0.98$). **C.** The characteristic association times from fits to the cumulative distributions for motors on single microtubules (blue bars) and bundles (red bars). Error bars represent the uncertainty in the fit parameters. **D.** Normalized probability distributions of the run lengths for kinesin motors on single microtubules (blue bars) and parallel bundles (red bars). Bin size is 0.5 μm. The fit to times greater than 1 μm is an exponential decay $y = A^*\exp(x/x_0)$, where A is the amplitude and x_0 is the characteristic run length. The best fits for the kinesin motors on single microtubules (blue line, $A = 2.3 \pm 0.3$, $x_0 = 0.65 \pm 0.04$ s, $R^2 = 0.97$) and parallel bundles (red lines, $A = 1.95 \pm 0.4$, $x_0 = 0.68 \pm 0.07$, $R^2 = 0.98$) are shown. **E.** Normalized cumulative distributions of the run length of kinesin motors on single microtubules (blue squares) and parallel bundles (red markers). Cumulative distributions data were fit using Eq. (1) and best fits for motors on single microtubules (blue line, $A = 1.56 \pm 0.09$, $x_0 = 1.00 \pm 0.01$ μm, $R^2 = 0.98$) and parallel bundles (red line, $A = 1.51 \pm 0.03$; $x_0 = 0.92 \pm 0.02$ μm, $R^2 = 0.96$). **F.** The characteristic run lengths from fits to the cumulative distributions for motors on single microtubules (blue bars) and bundles (red bars). Error bars represent the uncertainty in the fit parameters. [Color figure can be viewed in the online issue, which is available at wileyonlinelibrary.com.]

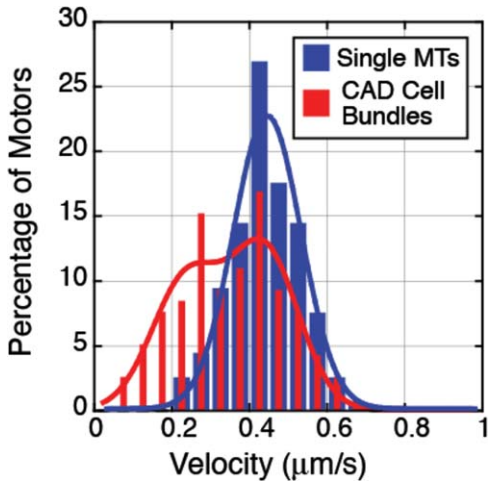

Fig. 3. Velocity distribution for motors on single microtubules compared to parallel bundles from CAD cells. Normalized probability distribution of the velocities of kinesin motors on single microtubules (blue bars, $N = 160$) and parallel bundles (red bars, $N = 122$). Velocity distribution for motors on single microtubules is best fit by a single Gaussian as in Eq. (2) (blue line, $A = 0.23 \pm 0.01$, $x_0 = 0.439 \pm 0.005$ μm/s, $\sigma = 0.087 \pm 0.005$ μm/s, $R^2 = 0.96$). Velocity distribution for motors on parallel bundles is best fit by a sum of two Gaussians (red line, $A = 0.12 \pm 0.03$, $x_1 = 0.44 \pm 0.05$ μm/s, $\sigma_1 = 0.087 \pm 0.03$ μm/s, $B = 0.10 \pm 0.03$, $x_2 = 0.24 \pm 0.06$ μm/s, $\sigma_2 = 0.090 \pm 0.04$ μm/s, $R^2 = 0.91$). [Color figure can be viewed in the online issue, which is available at wileyonlinelibrary.com.]

(66%; Fig. 4B; Supporting Information Table 1). For all our data in the presence of PEG, we will compare the results for kinesin motility on bundles to the motility on single microtubules in the presence of PEG at the same concentration.

We found that the percentage of motors that pause during a run on bundles (57% ± 5%) was higher compared to the percentage that pause on single microtubules in the presence of PEG (43% ± 5%), and this difference was larger than the uncertainty in each measurement (Fig. 4C; Supporting Information Table 1).

To examine motor reversal, we defined a reversal as a displacement >209 nm in the direction opposite of the prior displacements, and this alternate direction displacement must have persisted for at least two frames. We estimated the uncertainty in the percentage of motors that reversed as the standard error of proportion. We found that significantly more motors reverse on bundles (34% ± 5%) than on single microtubules in the presence of PEG (8% ± 2%), and this difference was larger than the uncertainty in each measurement (Fig. 4C; Supporting Information Table 1). We hypothesize that motor reversals are caused by motors that dissociate from one microtubule and reassociate to another microtubule within the bundle but with the opposite polarity. Below, we test this mechanism using a simulation.

We calculated the velocity of the motile segments for all motors. For motors that reverse, the speed (absolute value of velocity) of the individual segments was averaged to give an average speed for the entire run. Kinesin-1 motor speed was affected by the presence of PEG and by bundling (Fig. 4D). Motors on single and bundled microtubules displayed bimodal distributions best fit by a sum of two Gaussian distributions (Eq. (2); Fig. 4D). For the motors on single microtubules, the fast population traveled at 0.418 ± 0.009 μm/s, and the slow population traveled at 0.239 ± 0.007 μm/s. When we examined the speeds of kinesin motors on bundles, we also see a fast (0.250 ± 0.007 μm/s) and a slow (0.100 ± 0.003 μm/s) population (Fig. 4D; Supporting Information Table 1). We do not observe many motors traveling at the highest speeds around 0.4 μm/s, as we observed for single microtubules and parallel bundles (Fig. 3; Supporting Information Table 1).

We quantified the association times of kinesin motors on single microtubules with PEG present and microtubule bundles created with PEG (Fig. 5). The total association time was measured as the total time a motor remained bound to the microtubule or bundle. We use the cumulative probability distribution and fit to a single exponential decay (Eq. (1); Fig. 5A). The fit equation did not fit the experimental data well at long times and systematically overestimated the data. In order to fit the data better, we used a fit that was a sum of two exponential decays:

$$y = 1 - A\exp\left(-\frac{x}{x_1}\right) - B\exp\left(-\frac{x}{x_2}\right) \qquad (3)$$

where A and B are amplitudes and x_1 and x_2 are different characteristic decay constants (Fig. 5A). For a single data set fit with the double exponential decay, the two decay constants were distinct by a factor of five or six. Using the double decay fit (Eq. (3)), we determined the characteristic decay times (long and short times, Fig. 5B). We find both short and long times were longer on bundles by a factor of two, and this difference was larger than the uncertainty of either measurement (Fig. 5B; Supporting Information Table 1).

Because we have a population of motors that reverse and a population that only move unidirectionally, we can compare the association times of these populations. Nonreversing motors are best fit with a double exponential decay (Eq. (3)), but the motors that reverse are best fit with a single decay that only has a long-time decay constant (Figs. 5B and 5C). Using the best fits to each data set, we determined the characteristic decay times and the uncertainty to compare nonreversing and reversing motors (Supporting Information Fig. 1A, Table 1).

Due to the motor's ability to reverse direction on bundles, the run lengths can be long and complicated, with switchbacks (Fig. 6A). We devised several different metrics to assess the run lengths to compare between motors on single microtubules and bundles with PEG (Fig. 6A). First, we measured the total distance the motor translocated, which is a sum of all displacements regardless of the direction:

$$R_{\text{total}} = \sum_i |\Delta x|_i \quad (4)$$

where R_{total} is the total run length, Δx_i is the run length of a unidirectional segment of motion (s_i), and the sum is performed over all segments, i (Fig. 6A). For motors that reverse directions during a run, the total run length was the sum of the absolute value of the displacements of each segment of the run (Fig. 6A). Second, we measured the total displacement of single motors, Δx_{total}, on bundles, regardless of direction (absolute value, Fig. 6A). For motors that move in a single direction, this is the same distance as R_{total}.

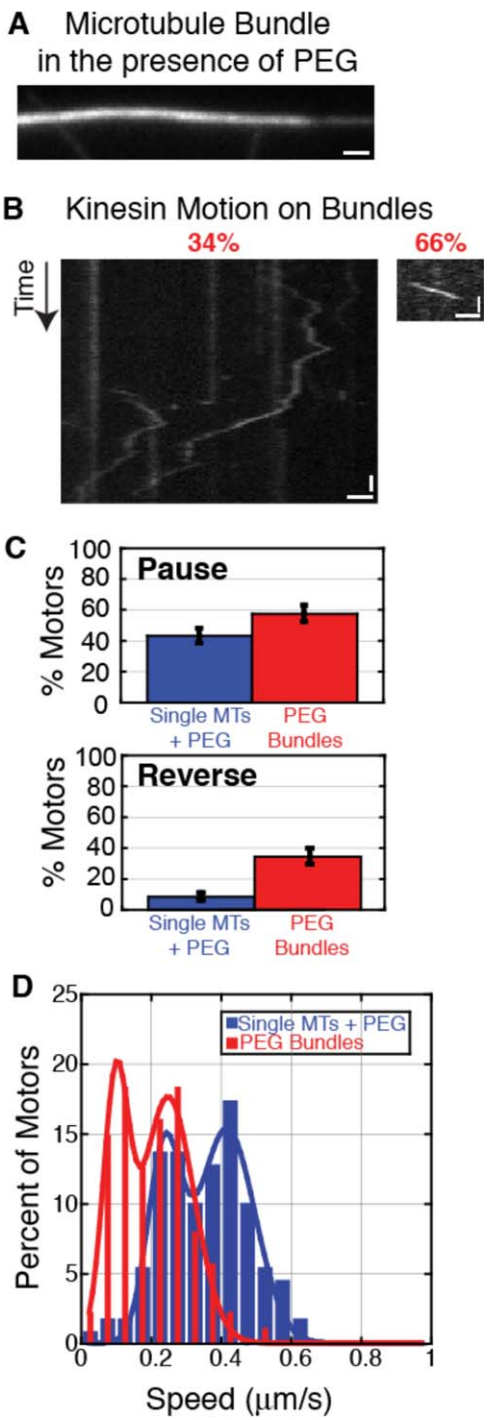

For motors that reverse direction, this is the distance between where the motor landed on the microtubule and where the motor finally dissociated from the microtubule (Fig. 6A).

We found that motors on bundles traveled shorter total distances (R_{total}) compared to motors on single microtubules (Fig. 6B). The total displacement (Δx_{total}) of motors traveling on bundles was shorter still (Fig. 6B), as expected since motors that reverse direction spend time walking back to their starting position. We fit the cumulative probability distributions to single exponential decays (Eq. (1)) to determine the characteristic decay times (Fig. 6B). The run length distributions are always best fit by a single exponential decay (Eq. (1)). From the fits, the total run length is shorter on bundles (1.84 ± 0.03 μm) compared to run lengths on single microtubules (2.28 ± 0.03 μm). The total displacement has an even shorter characteristic decay length (1.37 ± 0.02 μm; Fig. 6C; Supporting Information Table 1).

We can compare the total run lengths for motors that did not reverse (nonreversing) to those that did reverse direction (reversing; Fig. 6C). We also measured the individual segment (s_i) run lengths, and we can compare those displacements to the total run lengths (Fig. 6C). Comparing these three metrics, we find that each cumulative distribution plot is best fit by a single exponential decay (Supporting Information Fig. 1B), as the other run length distributions. For nonreversing motors, the run length is 40% shorter than motors on single microtubules (Fig. 6C; Supporting Information Table 1). Reversing motors have significantly longer run lengths than nonreversing motors, but the total run length is only 17% longer than motors on single microtubules. If we examine the segments of motor trajectories that reverse, we see that motors move only 0.85 ± 0.01 μm before switching direction, significantly shorter than the run length on a single microtubule

Fig. 4. Motors walking on microtubule bundles made using crowding by PEG can reverse. **A.** Representative image of microtubules bundled with PEG. Scale bar is 1 μm. **B.** Representative kymographs of motors walking along microtubules bundled with PEG show reversing (34%) and nonreversing (66%) motors. Horizontal scale bars are 1 μm, vertical scale bars are 5 s. **C.** The percentage of motors that pause (top) and reverse (bottom) on single microtubules (blue bars) and bundles (red bars) in the presence of PEG. Error bars represent the standard error of proportion. **D.** Normalized probability distribution of the speeds of kinesin motors on single microtubules in the presence of PEG (blue bars, $N = 109$) and PEG bundles (red bars, $N = 87$). The speed of motors walking on single microtubules with PEG are best fit by a double Gaussian (blue line, $A = 0.153 \pm 0.009$, $x_1 = 0.4180 \pm 0.009$ μm/s, $\sigma_1 = 0.11 \pm 0.01$ μm/s, $B = 0.13 \pm 0.01$, $x_2 = 0.239 \pm 0.009$ μm/s, $\sigma_2 = 0.0676 \pm 0.009$ μm/s, $R^2 = 0.97$). Speed distribution for motors on bundles is best fit by a sum of two Gaussians (red line, $A = 0.176 \pm 0.008$, $x_1 = 0.250 \pm 0.007$ μm/s, $\sigma_1 = 0.105 \pm 0.009$ μm/s, $B = 0.17 \pm 0.01$, $x_2 = 0.100 \pm 0.003$ μm/s, $\sigma_2 = 0.051 \pm 0.007$ μm/s, $R^2 = 0.98$). [Color figure can be viewed in the online issue, which is available at wileyonlinelibrary.com.]

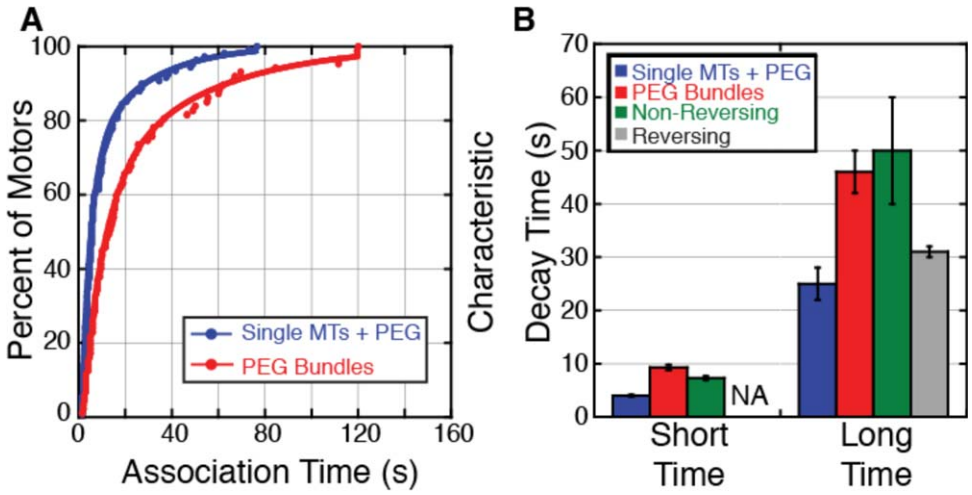

Fig. 5. Association times of kinesin motors to single microtubules and random-polarity bundles in the presence of PEG. **A.** Normalized cumulative distribution of kinesin motor association times to single microtubules (blue circles, $N = 109$) and bundles (red circles, $N = 87$) in the presence of PEG. Distributions are best fit to a sum of two exponentials (Eq. (3)) for association times on single microtubules (blue line, $A = 1.00 \pm 0.03$, $x_1 = 4.0 \pm 0.2$ s, $B = 0.32 \pm 0.04$, $x_2 = 25 \pm 3$ s, $R^2 = 0.995$) and bundles (red line, $A = 0.73 \pm 0.03$, $x_1 = 9.3 \pm 0.5$ s, $B = 0.41 \pm 0.04$, $x_2 = 46 \pm 4$ s, $R^2 = 0.998$). **B.** The characteristic decay times (short and long) of the cumulative distribution data sets for kinesin motors on single microtubules (blue bars) and bundles (red bars). For motors on bundles, we separately display the characteristic decay times for motors that do not reverse (green bars) and those that do reverse (gray bars). Error bars represent the uncertainty in the fit parameters. [Color figure can be viewed in the online issue, which is available at wileyonlinelibrary.com.]

(Fig. 6C; Supporting Information Fig 1, Table 1). Thus, although the reversing motors have a longer total distance, these trajectories are composed of about three to four directional switches of much shorter runs.

Motility on Antiparallel Bundles With Intermicrotubule Spacing

Close-packed bundles made with PEG significantly hindered forward motion of motors compared to translocation on single microtubules. We sought to investigate the effects of MAPs within bundles: Are MAPs roadblocks or could they act as spacers to prevent a greater obstacle formed by close-packed microtubules? MAPs have been shown to be obstacles or roadblocks to forward motion in experiments with single microtubules [Dixit et al., 2008]. On the other hand, there is evidence that MAPs could also space apart microtubules in the bundle, so they could rescue motion on the close-packed bundles. We utilized a MAP known to space apart bundled microtubules, MAP65. MAP65-1 is a plant analog to Ase1 and PRC1. Ase1 and PRC1 are used in mitosis to create the antiparallel interpolar array of microtubules in the spindle [Chan et al., 1999; Gaillard et al., 2008]. In plants, MAP65-1 acts to align dynamic microtubules in the plant cell cortex [Tulin et al., 2012].

We made two types of bundles with MAP65-1: bundles with MAP65 alone and bundles with MAP65 and PEG together. We compared kinesin-1 motility on bundles to motility on single microtubules in the presence of either MAP65 alone or MAP65 and PEG together. These experimental conditions served as controls to account for the effects of MAP65 with or without PEG. We determined that bundles had in average 16 microtubules (Fig. 7A).

Both types of bundles with MAP65 (with and without PEG) induced reversals of motors (Fig. 7B). We quantified the percentage of motors that reversed and found that significantly more motors reversed on bundles compared to similar conditions on single microtubules (Fig. 7C). We found a lower percentage of motors paused on single microtubules in the presence of MAP65 alone (Fig. 7C). Motors on single microtubules in the presence of both MAP65 and PEG or on bundles of either type all displayed similar, higher likelihoods for pausing during a run (Fig. 7C).

We found the speeds of motors were not affected by bundling with MAP65 (Fig. 7D). The two distributions were both bimodal with fast populations (single microtubules: 0.31 ± 0.03 μm/s, bundles: 0.32 ± 0.03 μm/s) and slow populations (single microtubules: 0.14 ± 0.03 μm/s, bundles: 0.160 ± 0.008 μm/s; Fig. 7D; Supporting Information Table 1). Interestingly, motors with either MAP65 or PEG both display bimodal distributions, which we never observe for motor on single microtubules in the absence of any additive (Supporting Information Fig. 2).

The speeds of motors in the presence of PEG and MAP65 were both bimodal (Fig. 7E). The addition of PEG had little effect on the velocity of motors on single microtubules compared to MAP65 alone. Both distributions had similar fast populations (0.36 ± 0.05 μm/s) and slow populations (0.176 ± 0.009 μm/s; Fig. 7E compared to Fig. 7D). Motors on bundles had an altered distribution of speeds where the mean velocities for the fast population (0.293 ± 0.009 μm/s) and slow population

(0.25 ± 0.09 μm/s) are intermediate (Fig. 7E; Supporting Information Table 1).

The association time of motors on single microtubules in the presence of MAP65 displayed a single exponential decay (Eq. (1)) with a short characteristic time (Figs. 8A and 8B). Motors on bundles had two characteristic decay times (Eq. (3)), and the short time was similar to motors on single microtubules (Figs. 8A and 8B). Motors on single microtubules or bundles with MAP65 and PEG displayed two characteristic association times (Eq. (3); Figs. 8A and 8C). The shorter characteristic time was similar between single microtubules and bundles, but the longer characteristic time was 50% higher on bundles compared to single microtubules (Fig. 8C; Supporting Information Table 1).

We compared the association times for motors that do not reverse to those that do reverse and plot these characteristic times as a bar chart (Figs. 8B and 8C, see Supporting Information Fig. 3A for distributions with best fits). In the presence of MAP65, the short time association time for nonreversing motors on bundles is the same as motors on single microtubules (Fig. 8B; Supporting Information Table 1). The long time is about 2–3 times larger than the short time (Fig. 8B; Supporting Information Table 1). Motors that reverse on bundles with MAP65 display only a single, long characteristic time that is four times longer than the time constant for single microtubules (Fig. 8B; Supporting Information Table 1), implying that the subset of reversing motors are able to stay bound to the bundle for significantly longer. Given that the control experiments never display such long association times, our data imply that longer associations are likely caused by the bundle architecture.

We observed similar trends for the motors moving on bundles with both MAP65 and PEG. In agreement with the PEG-only data (Fig. 5), motors in the presence of PEG and MAP65 on single microtubules display two characteristic association times (Figs. 8A and 8C). Motors on bundles also have two association times (Figs. 8A and 8C), but the long time is 50% longer on bundles compared to single microtubules (Figs. 8A and 8C; Supporting Information Table 1). Motors on bundles that never reverse and those that reversed each displayed only a single characteristic

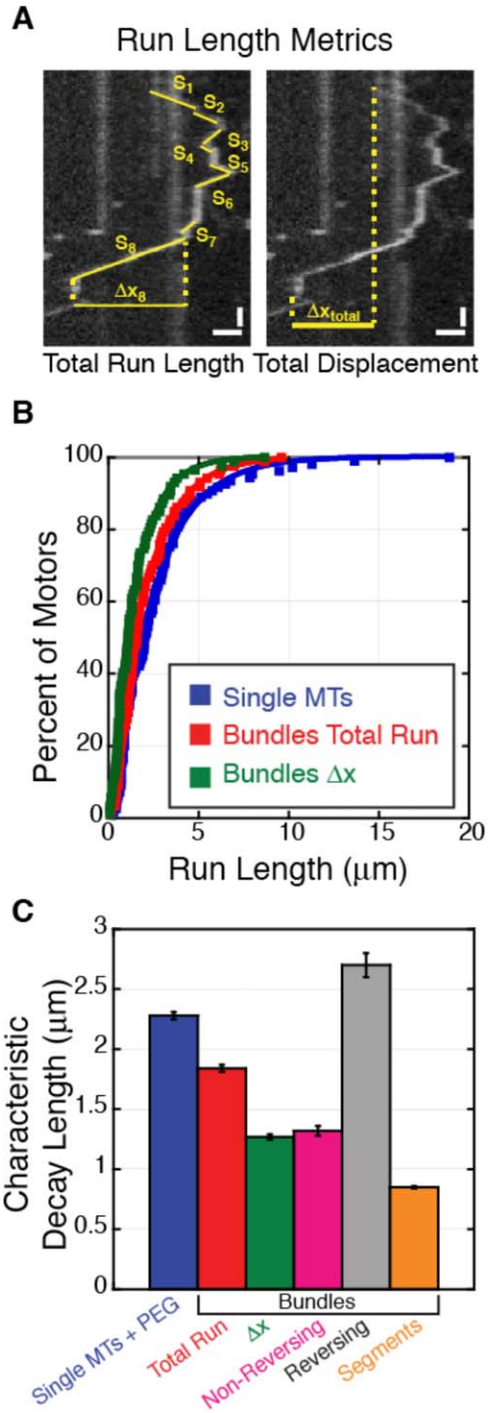

Fig. 6. Metrics to quantify the run length of motors on random bundles made with PEG. **A.** Kymograph of a reversing motor with the individual unidirectional segments, s_i, marked. Each segment, s_i has a segment displacement run length, Δx_i. The total run length, R_{total}, is the sum of the absolute value of all individual segments. The total displacement of the motor, Δx, is the distance the motor goes from the initial association to the final dissociation. Horizontal scale bars are 1 μm, vertical scale bars are 5 s. **B.** The run lengths of motors on single microtubules with PEG (blue squares, $N = 109$), total run length (red squares, $N = 87$) and total displacement (green squares, $N = 87$) on bundles in the presence of PEG. The best fit for run lengths on single microtubules is a single exponential, Eq. (1) (blue line, $A = 1.155 \pm 0.008$, $x_0 = 2.28 \pm 0.03$ μm, $R^2 = 0.99$). The best fit for total run lengths on bundles is a single exponential (red line, $A = 1.16 \pm 0.01$, $x_0 = 1.84 \pm 0.03$ μm, $R^2 = 0.99$). The best fit for total displacement on bundles is a single exponential (green line, $A = 1.086 \pm 0.008$, $x_0 = 1.37 \pm 0.02$ μm, $R^2 = 0.99$). **C.** The characteristic decay times of the cumulative distribution data sets for kinesin motors on single microtubules (blue bars) and bundles. For motors on bundles, we separately display the characteristic decay times for the total run length (red bars), total displacement, Δx, (green bars), motors that do not reverse (fushia bars) those that do reverse (gray bars) and the unidirectional segments of the reversing motors (orange bars). Error bars represent the uncertainty in the fit parameters. [Color figure can be viewed in the online issue, which is available at wileyonlinelibrary.com.]

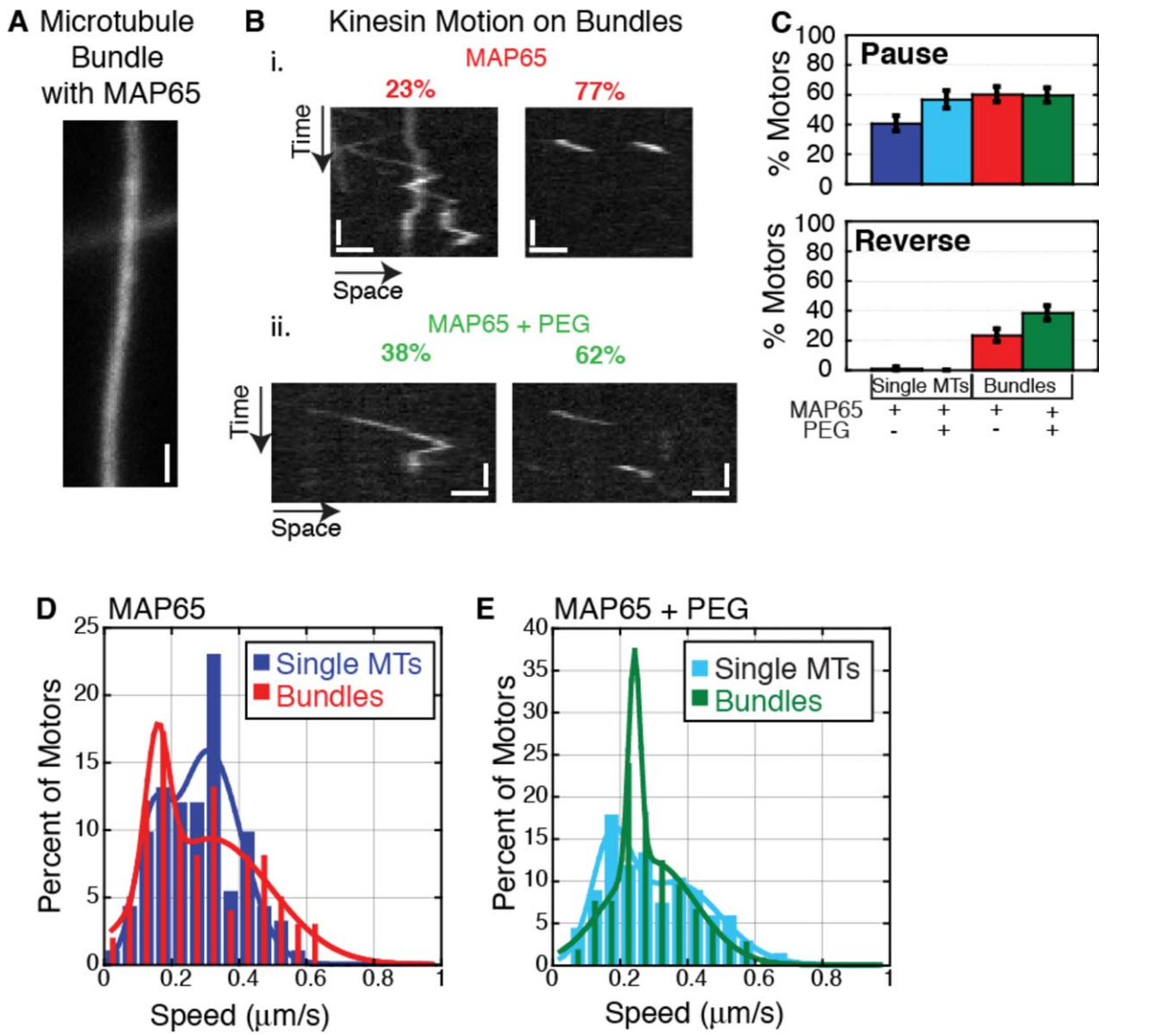

Fig. 7. Motor motility on bundles made with MAP65 or MAP65 and PEG. **A.** Representative image of microtubules bundled with MAP65. Scale bar is 1 μm. **B.** Representative kymographs of motors walking along microtubules bundled with (**i**) MAP65 or (**ii**) MAP65 and PEG. Horizontal scale bars are 1 μm, vertical scale bars are 5 s. **C.** The percentage of motors that pause (top) and reverse (bottom) on single microtubules with MAP65 (blue bars) and or MAP65 and PEG (light blue bars) or bundles with MAP65 (red bars) or MAP65 and PEG (green bars). Error bars represent the standard error of proportion. **D.** Normalized probability distribution of the speeds of kinesin motors on single microtubules (blue bars, $N = 91$) and bundles (red bars, $N = 98$) in the presence of MAP65. Motors walking on single microtubules are best fit by a double Gaussian (blue line, $A = 0.16 \pm 0.02$, $x_1 = 0.31 \pm 0.03$ μm/s, $\sigma_1 = 0.10 \pm 0.03$ μm/s, $B = 0.08 \pm 0.05$, $x_2 = 0.14 \pm 0.03$ μm/s, $\sigma_2 = 0.05 \pm 0.03$ μm/s, $R^2 = 0.84$). Speed distribution for motors on bundles is best fit by a sum of two Gaussians (red line, $A = 0.09 \pm 0.01$, $x_1 = 0.32 \pm 0.03$ μm/s, $\sigma_1 = 0.18 \pm 0.02$ μm/s, $B = 0.11 \pm 0.02$, $x_2 = 0.160 \pm 0.008$ μm/s, $\sigma_2 = 0.04 \pm 0.01$ μm/s, $R^2 = 0.91$). **E.** Normalized probability distribution of the speeds of kinesin motors on single microtubules (light blue bars, $N = 67$) and bundles (green bars, $N = 104$) in the presence of MAP65 and PEG. Motors walking on single microtubules are best fit by a double Gaussian (light blue line, $A = 0.108 \pm 0.009$, $x_1 = 0.36 \pm 0.05$ μm/s, $\sigma_1 = 0.16 \pm 0.02$ μm/s, $B = 0.11 \pm 0.02$, $x_2 = 0.172 \pm 0.007$ μm/s, $\sigma_2 = 0.034 \pm 0.006$ μm/s, $R^2 = 0.95$). Speed distribution for motors on bundles is best fit by a sum of two Gaussians (green line, $A = 0.123 \pm 0.009$, $x_1 = 0.293 \pm 0.009$ μm/s, $\sigma_1 = 0.132 \pm 0.008$ μm/s, $B = 0.24 \pm 0.09$, $x_2 = 0.25 \pm 0.09$ μm/s, $\sigma_2 = 0.01 \pm 0.2$ μm/s, $R^2 = 0.98$). [Color figure can be viewed in the online issue, which is available at wileyonlinelibrary.com.]

association time (Fig. 8C; see Supporting Information Fig. 3B for distributions with best fits). Nonreversing motors had a long time similar to the long time of motors on single microtubules. Reversing motors were associated for over twice as long as nonreversing motors (Fig. 8C; Supporting Information Table 1).

We quantified the run length for motors on single microtubules or bundles in the presence of MAP65 only or MAP65 and PEG. The run length distributions were single exponentials (Eq. (1)), and we used the characteristic run lengths to compare different experimental systems (single vs. bundle, MAP65 only, MAP65 and PEG) and different

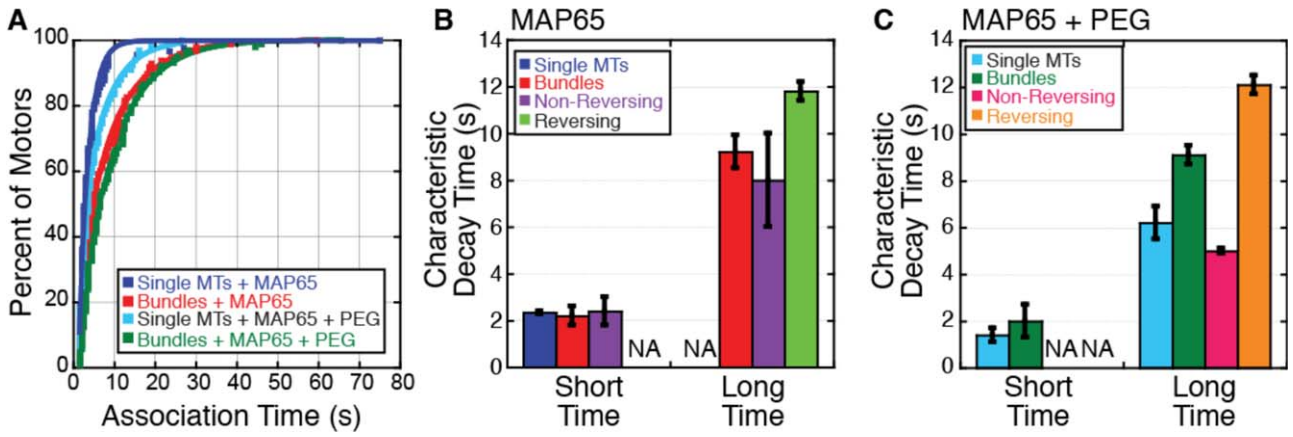

Fig. 8. Association time for kinesin motors on single microtubules or bundles with MAP65 or MAP65 and PEG. **A.** Normalized cumulative distributions for the association times for kinesin motors on single microtubules with MAP65 (blue squares, $N = 91$), bundles with MAP65 (red squares, $N = 98$), single microtubules with MAP65 and PEG (light blue squares, $N = 67$), and bundles with MAP65 and PEG (green squares, $N = 104$). The data of motors on single microtubules with MAP65 are best fit by a single exponential decay (blue line, Eq. (1), $A = 1.69 \pm 0.04$, $x_0 = 2.34 \pm 0.06$ s, $R^2 = 0.98$). The data of motors on bundles with MAP65 are best fit by a double exponential (red line, Eq. 3, $A = 0.58 \pm 0.06$, $x_1 = 2.2 \pm 0.4$ s, $B = 0.77 \pm 0.09$, $x_2 = 9.2 \pm 0.7$, $R^2 = 0.99$). The data of motors on single microtubules with MAP65 and PEG are best fit by a double exponential (light blue line, Eq 3, $A = 0.95 \pm 0.09$, $x_1 = 1.4 \pm 0.3$ s, $B = 0.8 \pm 0.1$, $x_2 = 6.2 \pm 0.7$, $R^2 = 0.99$). The data of motors on bundles with MAP65 and PEG are best fit by a double exponential (green line, Eq. 3, $A = 0.25 \pm 0.04$, $x_1 = 1.7 \pm 0.6$ s, $B = 1.04 \pm 0.04$, $x_2 = 9.0 \pm 0.3$, $R^2 = 0.996$). **B.** The characteristic decay times (short and long) to the cumulative distribution data sets for kinesin motors on single microtubules (blue bars) and bundles (red bars) in the presence of MAP65. For motors on bundles, we separately display the characteristic decay times for motors that do not reverse (violet bars) and those that do reverse (green bars). If the fit was a single exponential decay, we classified the characteristic time as either short or long to plot. Error bars represent the uncertainty in the fit parameters. **C.** The characteristic decay times (short and long) to the cumulative distribution data sets for kinesin motors on single microtubules (cyan bars) and bundles (green bars) in the presence of MAP65 and PEG. For motors on bundles, we separately display the characteristic decay times for motors that do not reverse (fusia bars) and those that do reverse (orange bars). If the fit was a single exponential decay, we classified the characteristic time as either short or long to plot. Error bars represent the uncertainty in the fit parameters. [Color figure can be viewed in the online issue, which is available at wileyonlinelibrary.com.]

populations of motors (nonreversing, reversing, segments; Fig. 9). In general, we found that motors traveling on bundles had longer total run lengths and total displacements compared to motors on single microtubules (Figs. 9B and 9C; see Supporting Information Figs. 3C and 3D for distributions with best fits). The population of motors that reversed traveled a factor of 2–3 farther than motors on single microtubules (Figs. 9B and 9C; Supporting Information Table 1). For reversing motors, the segments between reversals had similar characteristic run lengths as the run lengths of motors on single microtubules (Figs. 9B and 9C; Supporting Information Table 1), implying that reversing motors switch direction 2–3 times. Interestingly, the trends in the run length were very similar for the motors with MAP65 either in the presence or absence of PEG, and the main difference is that PEG slightly increased the run length of motors in all categories (Figs. 9B and 9C; Supporting Information Table 1).

Model of Dissociation and Re-association Mechanism for Reversals

For all three types of bundles where the polarity was mixed (PEG, MAP65, and MAP65 with PEG), we observed reversals. We hypothesize that the reversals we observed on all mixed polarity bundles are due to motors walking in a single direction on one of the microtubules of the bundle, dissociating and re-associating to the same bundle on a microtubule oriented with the opposite polarity. In order to test this mechanism of motor reversal, we modeled a particle moving with some simple rules: particles moved unidirectionally along a lattice of binding sites for a fixed time, after the fixed time, the particle could decide to continue in the same direction or switch to the opposite direction and move for the same set time. All velocities were constant at 300 nm/s, a velocity similar to kinesin motors in our assays. The probability of switching was 50% and the motors were never able to dissociate from the track (Fig. 10A).

Using this model, we created simulated trajectories of motors that appeared similar to the trajectories of our reversing kinesin motors in experiments (Fig. 10B). Although these trajectories appeared similar, we needed a metric to compare the simulated data to the experimental data. For the comparison, we calculated the time-averaged mean squared displacement (TA-MSD) [Tabei et al., 2013]. The TA-MSD can be seen as a moving average of displacement. We rescaled the data TA-MSD by dividing out the initial instantaneous velocity to remove differences due to different diffusion or velocity constants between individual motors, allowing us to average the data together from many motors.

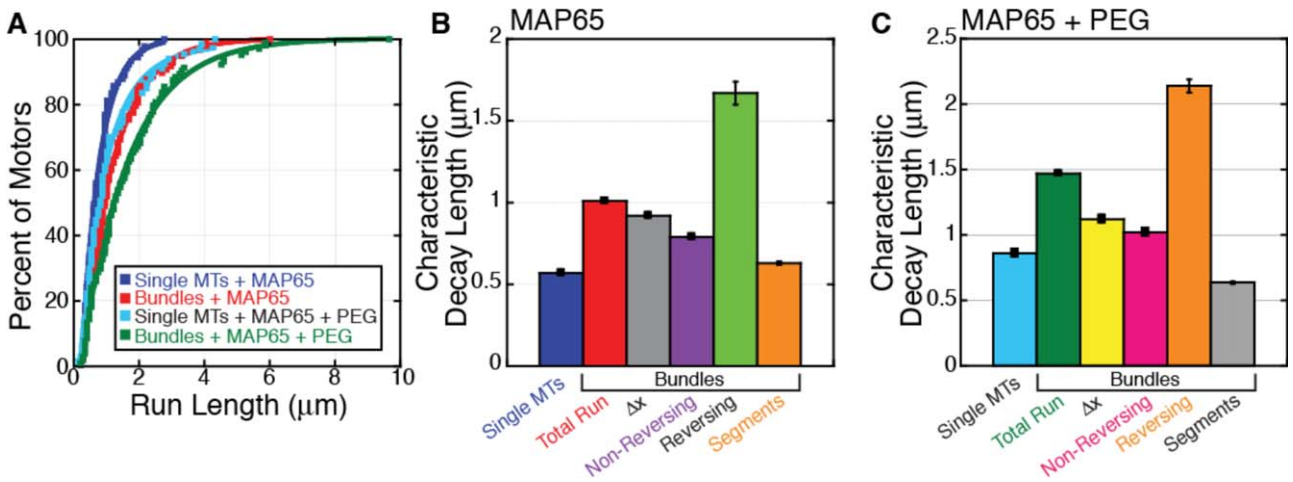

Fig. 9. Run lengths for kinesin motors on single microtubules or bundles with MAP65 or MAP65 and PEG. **A.** Normalized cumulative distributions for the total run lengths for kinesin motors on single microtubules with MAP65 (blue squares, $N = 91$), bundles with MAP65 (red squares, $N = 98$), single microtubules with MAP65 and PEG (light blue squares, $N = 67$), and bundles with MAP65 and PEG (green squares, $N = 104$). The data of motors on single microtubules with MAP65 are best fit by a single exponential decay (blue line, Eq. (1), $A = 1.56 \pm 0.02$, $x_0 = 0.57 \pm 0.01$ s, $R^2 = 0.99$). The data of motors on bundles with MAP65 are best fit by a single exponential (red line, Eq. (1), $A = 1.269 \pm 0.008$, $x_0 = 1.011 \pm 0.009$ s, $R^2 = 0.997$). The data of motors on single microtubules with MAP65 and PEG are best fit by a single exponential (Eq. (1), $A = 1.25 \pm 0.02$, $x_0 = 0.86 \pm 0.02$, $R^2 = 0.99$). The data of motors on bundles with MAP65 and PEG are best fit by a single exponential (green line, Eq. (1), $A = 1.170 \pm 0.006$, $x_0 = 1.47 \pm 0.01$ s, $R^2 = 0.996$). **B.** The characteristic decay times of the cumulative distribution data sets for kinesin motors on single microtubules (blue bars) and bundles in the presence of MAP65. For motors on bundles, we separately display the characteristic decay times for the total run length (red bars), total displacement, Δx, (gray bars), motors that do not reverse (violet bars) those that do reverse (green bars) and the unidirectional segments of the reversing motors (orange bars). Error bars represent the uncertainty in the fit parameters. **C.** The characteristic decay times of the cumulative distribution data sets for kinesin motors on single microtubules (light blue bars) and bundles in the presence of MAP65 and PEG. For motors on bundles, we separately display the characteristic decay times for the total run length (green bars), total displacement, Δx, (yellow bars), motors that do not reverse (fushia bars) those that do reverse (orange bars) and the unidirectional segments of the reversing motors (gray bars). Error bars represent the uncertainty in the fit parameters. [Color figure can be viewed in the online issue, which is available at wileyonlinelibrary.com.]

We calculated the TA-MSD for simulated particles that could decide to switch direction after seven-time steps (Fig. 10C) and compared it to the TA-MSD for motors walking on bundles made with PEG, MAP65, and MAP65 with PEG (Figs. 10D–10F). We saw similar trends between the motors on bundles made with MAP65 and the model (Figs. 10E and 10F), but motors on close-packed bundles made with PEG displayed trends in the TA-MSD that were dissimilar to the model data and the MAP65 bundle data (Fig. 10D). Our results suggest that the mechanism of reversals for motors on bundles made with MAP65 is likely dissociation followed by subsequent re-association of motors to an oppositely-oriented microtubule within the bundle. Our model does not recapitulate the data for the PEG bundles, possibly due to restricted motion within the close-packed bundles.

Discussion

We have investigated the effects of bundle polarity and spacing between microtubules on the motility of single kinesin-1 motors by creating different types of microtubule bundles. From these studies, we showed surprising and novel results in regard to motor transport on different bundle architectures. First, we show that parallel bundles with many binding sites are not able to enhance the association time or run length of kinesin-1 motor proteins. This could have implications for the long-distance transport of cargos along the parallel microtubule bundles in the axon. Although we know that multiple motors often carry cargos, we believe studying the effects on single kinesin-1 motors is relevant. Theoretical models of multiple motors carrying cargos show that the run lengths should be extremely long [Klumpp et al., 2005; Beeg et al., 2008]. Yet, no multimotor experiment has ever recapitulated these results [Conway et al., 2012; Derr et al., 2012; Jamison et al., 2012; Xu et al., 2013]. One hypothesis is that kinesin-1 motors could trade off on the load. Thus, the run length and association time would be elongated, but not as long as predicted by previous models. The longer association times are likely due to the fact that a second kinesin-1 is nearby and large cargos have a slow diffusion coefficient, allowing another motor to reattach and continue to carry the cargo before the entire complex diffuses away. These experimental results imply that it is still relevant and important to understand how single motors transport along microtubules in increasingly complex scenarios. Future studies of cargo transport with the same or different types of motors along bundles would be interesting to compare to single motors.

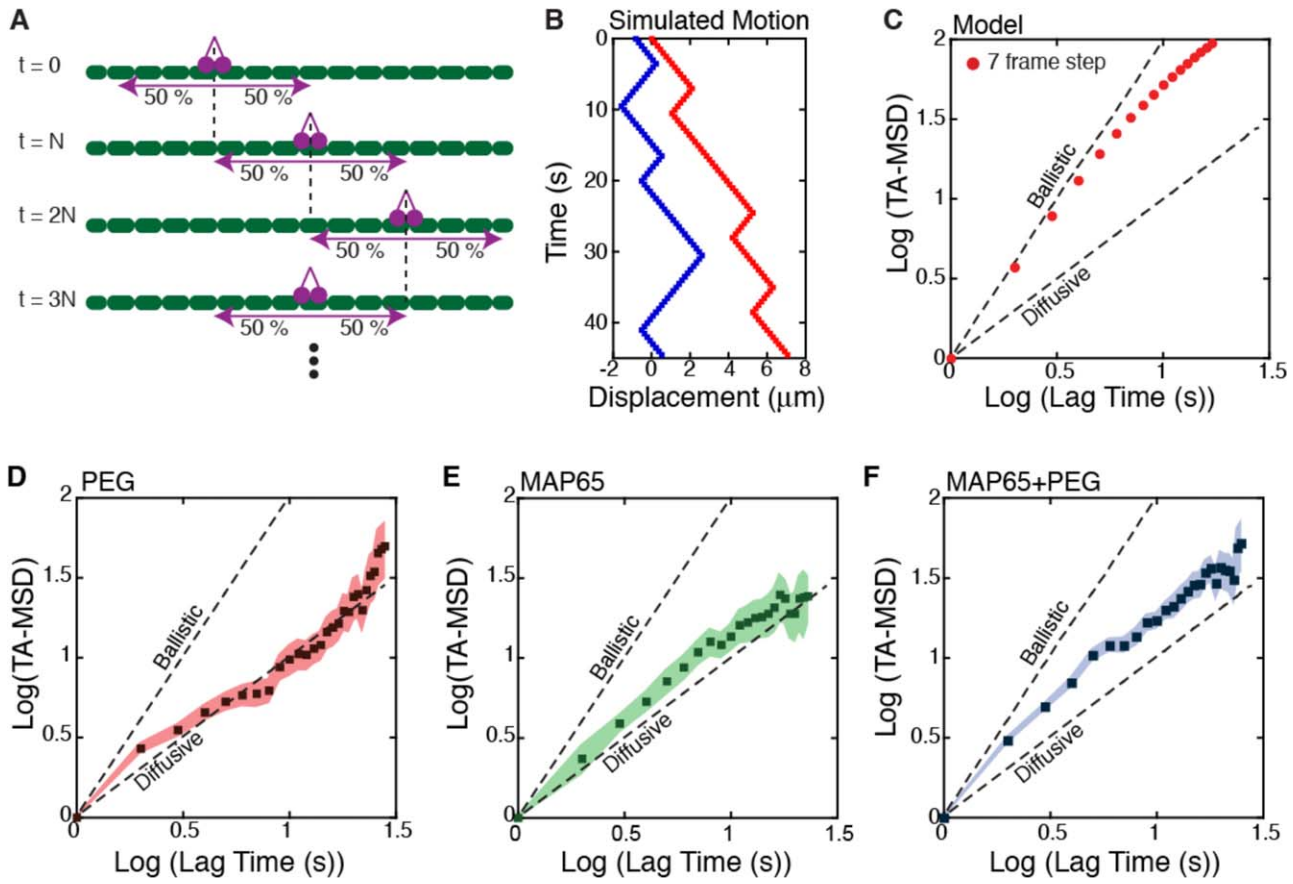

Fig. 10. Model and comparison to kinesin motility on bundles with PEG, MAP65, and MAP65 and PEG together. **A.** Cartoon describing the simulated data of motors walking on a one-dimensional bundle assumes that each time the motor walks, it goes a set distance, or, equivalently, a fixed time with a fixed velocity. After that run, the motor randomly chooses a new direction (left or right) with a 50% probability of choosing either. **B.** Simulated trajectories with run times before deciding a new direction of seven frames for two particles (red or blue squares). Plot has time origin in the top, left corner for easy comparison to kymographs in other figures. **C.** Plot of the log of the TA-MSD as a function of the log of the time for the simulated data sets. The TA-MSD is bilinear with an initial slope greater than one and a second slope approaching one. **D.** The log of the normalized TA-MSD plotted as a function of the log of the lag time for experimental trajectories on bundles made with PEG (dark red squares). The red shaded region represents the uncertainty of each point. **E.** The log of the normalized TA-MSD plotted as a function of the log of the lag time for experimental trajectories on bundles made with MAP65 (dark green squares). The green shaded region represents the uncertainty of each point. **F.** The log of the normalized TA-MSD plotted as a function of the log of the lag time for experimental trajectories on bundles made with MAP65 and PEG (dark blue squares). The blue shaded region represents the uncertainty of each point. [Color figure can be viewed in the online issue, which is available at wileyonlinelibrary.com.]

Next, we examined how a randomly-oriented bundle of microtubules made by crowding microtubules together with PEG can affect the motility of kinesin-1 motors. The motors were likely able to reverse direction during their run by associating to nearby, oppositely-oriented microtubules within the bundle, reducing the absolute displacement of motors from the beginning to the end of the association. Surprisingly, we found that the bundle itself inhibited motility of the motors causing shorter unidirectional runs and shorter segments within a trajectory for those motors that reversed direction compared to motors on single microtubules with PEG (Fig. 6). Additionally, motor velocity was slower on the bundles (Fig. 4). The likely mechanism for this inhibition is steric hindrance due to the neighboring microtubules of the bundle. Bundles made through crowding with PEG are close packed into hexagonal arrays (in cross-section). They are close enough to touch and would not allow motors to access the binding sites in those regions. If a kinesin-1 were to run into a microtubule blocking the next binding site, it has a high probability of dissociating, as shown by prior work [Dixit et al., 2008; Ross et al., 2008]. Dissociation could lead to re-association and a reversal or complete dissociation from the bundle.

In order to overcome the hindrance from closely-packed microtubules, we spaced microtubules apart using MAP65. We made bundles with MAP65 alone or MAP65 and PEG together. We find that the kinesin-1 motors on bundles in the presence of MAP65 recovered their run lengths, association times, and speeds, and the run length was further enhanced in the presence of PEG. Additionally, no decrease in motor speed was observed on MAP65 bundles compared to motors on single microtubules with MAP65, further

supporting the idea that MAPs can alleviate obstacles within the bundle by spacing apart microtubules.

Our data demonstrates that MAPs can act as spacers within microtubule bundles to allow motors more access to the microtubule surface. If the motor becomes trapped in the interstitial region of the bundle, which has many binding sites, the ability to reassociate and continue the run could be enhanced even further. Prior work showed that MAPs are obstacles to motor motion causing motors to dissociate [Seitz and Surrey, 2006; Vershinin et al., 2007; Dixit et al., 2008]. Recent data has shown that some MAPs may not act as obstacles at all, but speed bumps that slow down motors and MAP binding may be diffusive instead of stationary [McVicker et al., 2011; Xu et al., 2013; Lopez and Velntine, 2014]. Together with our results, we propose that MAPs function to space apart microtubules to give better access to the microtubule tracks.

In the cell, macromolecular crowding is high, and microtubule bundles would likely collapse into close-packed bundles due to depletion forces [Lodish et al., 2000; Sendek et al., 2014]. Indeed, we see interesting effects of PEG on the velocity and run length of single kinesin motors walking on single microtubules, which are worth studying. In particular, the velocity distributions for all experimental data in the presence of PEG are bimodal, and this could be due to the crowding on the motor binding. Electron micrographs of microtubule bundles in cells show significant space between the filaments [Hirokawa et al., 1988; Kanai et al., 1989; Chen et al., 1992; Chan et al., 1999; Gaillard et al., 2008]. Our data implies that MAPs could be important to enable motors to access microtubule tracks.

We used MAP65 in this study as a microtubule spacer. Future studies using MAP2 or tau would be interesting to test the effects of other MAPs as spacers. Indeed, we have previously shown that when tau binds to microtubules bundled with a crowding agent, the microtubules stay bundled, but the bundle loses contrast in differential interference contrast imaging [Ross et al., 2004].

We used a simple model to show that the reversals we observe are likely due to motors dissociating and reassociating to the bundle, but the model was not able to perfectly recapitulate the data and did not resemble the experimental data on PEG bundles. Future modeling work needs to be performed in order to fully understand what is occurring on these bundles.

Microtubules form amazingly complicated sets of arrays in cells depending on the cell type, stage of development, and position within the cell. Linear arrays, or bundles, are the simplest organization, yet they have a number of parameters that can affect their organization including the polarity of the microtubules within the bundle and the spacing between the microtubules. In this study, we have taken a bottom-up approach to understand how the simplest of multimicrotubule structures (bundles) can affect the long-range transport of single kinesin-1 motor proteins. Indeed, we find distinct differences in the motility metrics (association time, run length, velocity, and trajectory correlation (TA-MSD)) of single motors as an effect of the structure of the bundle. These assays provide important fundamental insights into the mechanisms by which the architecture of microtubule arrays controls motor transport. Specifically, the way you build your roads can dictate where and how far you travel.

Materials and Methods

Protein Purification

All protein purification procedures can be found in the supplemental methods.

Kinesin-1 Motility Assays on Single Microtubules

Assays were carried out in 10 μL flow chambers made of a glass slide attached to a cover slip with double-stick tape. Prior to use, cover slips were cleaned and treated with dimethyldichlorosilane solution, 2% w/v (GE Healthcare), as previously described [Conway et al., 2012]. Flow chambers were first incubated with 2% antitubulin antibody in PEM-100 for 5 min to attach microtubules, followed by a 5-min incubation with 5% Pluronic F-127 (Sigma) in PEM-100 to block the surface. Labeled microtubules (0.05 mg/mL microtubules, 20 μM Taxol in PEM-100) were allowed to bind for 10 min. Excess microtubules were removed with a wash step (10 mM dithiothreitol (DTT), 20 μM Taxol in PEM-100). Finally, motility mix was added to the chamber (2 nM green fluorescent protein (GFP) kinesin, 0.05% Pluronic F-127, 25 μM Taxol, 0.25 mg/mL bovine serum albumin (BSA), 50 mM DTT, 0.5 mM ATP, 15 mg/mL glucose, 0.5 mg/mL glucose oxidase, 0.15 mg/mL catalase in PEM-100). For motility on single microtubules in the presence of PEG, 5% PEG molecular weight (MW) 40,000 was added to the motility mix. For these assays, only 0.3 nM GFP-kinesin was added to the motility mix. For motility on single microtubules in the presence of MAP65, 112 nM MAP65 was added to the microtubule wash step and motility mix. For motility on single microtubules in the presence of MAP65 and PEG, 112 nM MAP65 and 5% PEG MW 40,000 were added to the motility mix. For these assays, only 0.3 nM GFP-kinesin was added to the motility mix.

Kinesin-1 Motility Assays on Parallel Microtubule Bundles

Parallel bundles were made from an immortalized CAD cell line (gift from K. Verhey). CAD cells were maintained in Dulbecco's modified eagle's medium (DMEM)/F12 (Gibco, 12400-024) media with 10% fetal bovine serum (FBS). To induce differentiation, CAD cells were plated on 20 mm glass bottom dishes (20,000–40,000 cells per plate) in DMEM/F12 plus 10% FBS. After cells adhered to the dish, cells were rinsed two times in DMEM/F12 without FBS.

Fresh DMEM/F12 media without FBS was added and the cells were left for 2–3 days to grow processes. To expose the microtubule cytoskeleton of differentiated CAD cells, a previously described protocol for studying the actin cytoskeleton was modified [Sivaramakrishnan and Spudich, 2009]. Differentiated cells were washed two times in 85% phosphate buffered saline (PBS), followed by exposure to Extraction Buffer (50 mM Imidazole, pH 6.8, 50 mM KCl, 0.5 mM $MgCl_2$, 0.1 mM ethylenediaminetetraacetic acid (EDTA), 1 mM ethylene glycol tetraacetic acid (EGTA), 50 mM Taxol, 1% Triton X-100, 4% 40,000 kD PEG) for 4 min. A Taxol solution (85% PBS with 50 μM Taxol) was added to the cells for 45 min to stabilize the microtubule cytoskeleton. Cells were then rinsed (1 mg/mL BSA, 50 μM Taxol in PEM-100) for 5 min. Finally, motility mix was added to the cells (0.7 nM GFP kinesin, 25 μM Taxol, 1 mg/mL BSA, 50 mM DTT, 0.5 mM ATP, 15 mg/mL glucose, 0.5 mg/mL glucose oxidase, 0.15 mg/mL catalase in PEM-100). For experiments where the microtubule cytoskeleton was observed with fluorescent Taxol, boron-dipyrromethene (BODIPY)-taxol was added at a tenth of the final Taxol concentration (5 μM BODIPY-taxol with 45 μM unlabeled taxol).

Kinesin-1 Motility Assays on PEG Microtubule Bundles

PEG microtubule bundles were made by mixing 0.45 μM polymerized microtubules with 5% (w/w) 40,000 kD PEG and 20 μM Taxol in PEM-100. Assays were carried out as described for motility assays on single microtubules with the only difference that PEG microtubule bundles were allowed to bind for 10 min and 5% PEG was included in the motility mix.

Kinesin-1 Motility Assays on MAP65 Microtubule Bundles

MAP65 microtubule bundles were made by mixing 0.45 μM polymerized microtubules with 112 nM MAP65 and 20 μM Taxol in PEM-100. Assays were carried out as described for motility assays on single microtubules except that MAP65 microtubule bundles were allowed to bind for 10 min and 112 nM MAP65 was included in the motility mix.

Kinesin-1 Motility Assays on MAP65 and PEG Microtubule Bundles

MAP65 microtubule bundles were made by mixing 0.45 μM polymerized microtubules with 112 nM MAP65 and 20 μM Taxol in PEM-100. Assays were carried out as described for MAP65 bundles except 5% PEG was added to the motility mix.

Image Acquisition

An image of the microtubules was acquired using epifluorescence prior to imaging GFP-kinesin motors. Two-minute recordings of kinesin motility were taken with a 500 ms exposure time using total internal reflection fluorescence microscopy with a 50 mW 488 nm Cyan laser (Spectra-Physics) illumination built around an inverted Nikon Ti-E microscope (Nikon). The microscope uses a Nikon 60× 1.49 numerical aperture (NA) objective and images were collected using an iXon electron multiplier charged-coupled device (CCD) camera (Andor) after a 4× beam expander. The final pixel size was 67.5 nm. Images were acquired at room temperature (25°C) with no delay using Nikon imaging system (NIS)-Elements and saved as nd2 files and exported as 16-bit tif files.

Image Analysis

We estimated the number of microtubules in bundles (N_{MTs}) by comparing the quantified average intensity of several single microtubules (I_{single}) to the intensity of the bundles (I_{bundle}) and dividing: $N_{MTs} = I_{bundle}/I_{single}$. Individual microtubules were imaged in separate chambers than bundles with the exact same imaging parameters (exposure time and illumination intensity) on the same day. The intensity of single microtubules and bundles were in the linear range of the camera detector.

Kinesin motility was analyzed using kymographs generated from the ImageJ plugin, MultipleKymograph. For velocity measurements, only the moving segments of runs were measured, so as to omit pauses from the overall velocity measurement. To determine the number of microtubules in PEG and MAP65 bundles, the fluorescence intensity of a single microtubule was compared to that of the microtubule bundle. Fluorescence intensity was determined by drawing a line perpendicular to the microtubule in ImageJ to create a plot profile. This data was fit to a Gaussian function in Kaleidagraph to determine the height of the fluorescence peak, which corresponds to the average fluorescence of the microtubule or microtubule bundle. The fluorescence intensity of a microtubule bundle was divided by the average fluorescence of a single microtubule to determine the number of microtubules within the bundle.

Simulation and TA-MSD Analysis

Detailed methods about the simulation and the TA-MSD analysis can be found in the supplemental methods section.

Acknowledgments

Thank you to Kristen Verhey for sending us the CAD cell line and for help with editing. Thank you to Patricia Wadsworth for use of her tissue culture facilities. Thank you to Ram Dixit for the MAP65 expression construct, and to Joshua Pringle and Amanda Tan for purification of the MAP65 protein. L. C., M. W. G., and J. L. R. were partially supported by NSF-DMR grant #1207783 to J. L. R. L. C. and M. W. G were partially supported by a grant from the Mathers Foundation. L. C. was supported

partially by the Institute for Cellular Engineering (ICE) IGERT to the University of Massachusetts led by Susan Roberts, DGE grant #0654128. M. W. G. was supported partially by the MRSEC on Polymers to the University of Massachusetts Amherst NSF-DMR grant #0820506. This work was also supported by Cottrell Scholar Grant #20031 from Research Corporation for Science Advancement.

References

Baas PW, Deitch JS, Black MM, Banker GA. 1988. Polarity orientation of microtubules in hippocampal neurons: uniformity in the axon and nonuniformity in the dendrite. Proc Natl Acad Sci USA 85:8335–8339.

Beeg J, Klumpp S, Dimova R, Gracià RS, Unger E, Lipowsky R. 2008. Transport of beads by several kinesin motors. Biophys J 94: 532–541.

Bisig CG, Chesta ME, Zampar GG, Purro SA, Santander VS, Arce CA. 2009. Lack of stabilized microtubules as a result of the absence of major maps in CAD cells does not preclude neurite formation. FEBS J 276:7110–7123.

Braak E, Braak H, Mandelkow EM. 1994. A sequence of cytoskeleton changes related to the formation of neurofibrillary tangles and neuropil threads. Acta Neuropathol 87:554–567.

Chan J, Jensen CG, Jensen LC, Bush M, Lloyd CW. 1999. The 65-kDa carrot microtubule-associated protein forms regularly arranged filamentous cross-bridges between microtubules. Proc Natl Acad Sci USA 96:14931–14936.

Chen J, Kanai Y, Cowan NJ, Hirokawa N. 1992. Projection domains of MAP2 and tau determine spacings between microtubules in dendrites and axons. Nature 360:674–677.

Chevalier-Larsen E, Holzbaur EL. 2006. Axonal transport and neurodegenerative disease. Biochim Biophys Acta 1762:1094–1108.

Conway L, Wood D, Tüzel E, Ross JL. 2012. Motor transport of self-assembled cargos in crowded environments. Proc Natl Acad Sci USA 109:20814–20819.

Derr ND, Goodman BS, Jungmann R, Leschziner AE, Shih WM, Reck-Peterson SL. 2012. Tug-of-war in motor protein ensembles revealed with a programmable DNA origami scaffold. Science 338: 662–665.

Dixit R, Ross JL, Goldman YE, Holzbaur EL. 2008. Differential regulation of dynein and kinesin motor proteins by tau. Science 319:1086–1089.

Gaillard J, Neumann E, Van Damme D, Stoppin-Mellet V, Ebel C, Barbier E, Geelen D, Vantard M. 2008. Two microtubule-associated proteins of Arabidopsis MAP65s promote antiparallel microtubule bundling. Mol Biol Cell 19:4534–4544.

Goldstein LS, Yang Z. 2000. Microtubule-based transport systems in neurons: the roles of kinesins and dyneins. Annu Rev Neurosci 23:39–71.

Hirokawa N, Takemura R. 2005. Molecular motors and mechanisms of directional transport in neurons. Nat Rev Neurosci 6:201–214.

Hirokawa N, Hisanaga S, Shiomura Y. 1988. MAP2 is a component of crossbridges between microtubules and neurofilaments in the neuronal cytoskeleton: quick-freeze, deep-etch immunoelectron microscopy and reconstitution studies. J Neurosci 8:2769–2779.

Hirokawa N, Niwa S, Tanaka Y. 2010. Molecular motors in neurons: transport mechanisms and roles in brain function, development, and disease. Neuron 68:610–638.

Jamison DK, Driver JW, Diehl MR. 2012. Cooperative responses of multiple kinesins to variable and constant loads. J Biol Chem 287:3357–3365.

Kanai Y, Takemura R, Oshima T, Mori H, Ihara Y, Yanagisawa M, Masaki T, Hirokawa N. 1989. Expression of multiple tau isoforms and microtubule bundle formation in fibroblasts transfected with a single tau cDNA. J Cell Biol 109:1173–1184.

Khatoon S, Grundke-Iqbal I, Iqbal K. 1992. Brain levels of microtubule-associated protein tau are elevated in Alzheimer's disease: a radioimmuno-slot-blot assay for nanograms of the protein. J Neurochem 59:750–753.

Klumpp S, Nieuwenhuizen TM, Lipowsky R. 2005. Self-organized density patterns of molecular motors in arrays of cytoskeletal filaments. Biophys J 88:3118–3132.

Li W, Xia JT, Feng Y. 2006. Microtubule stability and MAP1B upregulation control neuritogenesis in CAD cells. Acta Pharmacol Sin 27:1119–1126.

Lodish H, Berk A, Zipursky S. 2000. Molecular Cell Biology. New York: W. H. Freeman.

Lopez BJ, Velntine MT. 2014. Mechanical effects of EB1 on microtubules depend on GTP hydrolysis state and the presence of paclitaxel. Cytoskeleton (Hoboken), in press.

Massiera G, Van Citters KM, Biancaniello PL, Crocker JC. 2007. Mechanics of single cells: rheology, time dependence, and fluctuations. Biophys J 93:3703–3713.

McVicker DP, Chrin LR, Berger CL. 2011. The nucleotide-binding state of microtubules modulates kinesin processivity and the ability of Tau to inhibit kinesin-mediated transport. J Biol Chem 286:42873–42880.

Muresan V, Muresan Z. 2012. A persistent stress response to impeded axonal transport leads to accumulation of amyloid-β in the endoplasmic reticulum, and is a probable cause of sporadic Alzheimer's disease. Neurodegener Dis 10:60–63.

Needleman DJ, Ojeda-Lopez MA, Raviv U, Miller HP, Wilson L, Safinya CR. 2004. Higher-order assembly of microtubules by counterions: from hexagonal bundles to living necklaces. Proc Natl Acad Sci USA 101:16099–16103.

Perlson E, Maday S, Fu MM, Moughamian AJ, Holzbaur EL. 2010. Retrograde axonal transport: pathways to cell death? Trends Neurosci 33:335–344.

Qi Y, Wang JK, McMillian M, Chikaraishi DM. 1997. Characterization of a CNS cell line, CAD, in which morphological differentiation is initiated by serum deprivation. J Neurosci 17:1217–1225.

Reed NA, Cai D, Blasius TL, Jih GT, Meyhofer E, Gaertig J, Verhey KJ. 2006. Microtubule acetylation promotes kinesin-1 binding and transport. Curr Biol 16:2166–2172.

Ross JL, Santangelo CD, Makrides V, Fygenson DK. 2004. Tau induces cooperative Taxol binding to microtubules. Proc Natl Acad Sci USA 101:12910–12915.

Ross JL, Shuman H, Holzbaur EL, Goldman YE. 2008. Kinesin and dynein-dynactin at intersecting microtubules: motor density affects dynein function. Biophys J 94:3115–3125.

Seitz A, Surrey T. 2006. Processive movement of single kinesins on crowded microtubules visualized using quantum dots. EMBO J 25: 267–277.

Sendek A, Fuller HR, Hayre NR, Singh RR, Cox DL. 2014. Simulated cytoskeletal collapse via tau degradation. PLoS One 9:e104965.

Sivaramakrishnan S, Spudich JA. 2009. Coupled myosin VI motors facilitate unidirectional movement on an F-actin network. J Cell Biol 187:53–60.

Stepanova T, Slemmer J, Hoogenraad CC, Lansbergen G, Dortland B, De Zeeuw CI, Grosveld F, van Cappellen G, Akhmanova A,

Galjart N. 2003. Visualization of microtubule growth in cultured neurons via the use of EB3-GFP (end-binding protein 3-green fluorescent protein). J Neurosci 23:2655–2664.

Tabei SM, Burov S, Kim HY, Kuznetsov A, Huynh T, Jureller J, Philipson LH, Dinner AR, Scherer NF. 2013. Intracellular transport of insulin granules is a subordinated random walk. Proc Natl Acad Sci USA 110:4911–4916.

Tulin A, McClerklin S, Huang Y, Dixit R. 2012. Single-molecule analysis of the microtubule cross-linking protein MAP65-1 reveals a molecular mechanism for contact-angle-dependent microtubule bundling. Biophys J 102:802–809.

Vale RD. 2003. The molecular motor toolbox for intracellular transport. Cell 112:467–480.

Verhey KJ, Meyer D, Deehan R, Blenis J, Schnapp BJ, Rapoport TA, Margolis B. 2001. Cargo of kinesin identified as JIP scaffolding proteins and associated signaling molecules. J Cell Biol 152:959–970.

Vershinin M, Carter BC, Razafsky DS, King SJ, Gross SP. 2007. Multiple-motor based transport and its regulation by Tau. Proc Natl Acad Sci USA 104:87–92.

Xu J, King SJ, Lapierre-Landry M, Nemec B. 2013. Interplay between velocity and travel distance of kinesin-based transport in the presence of tau. Biophys J 105:L23–L25.